Plastic deformation and development of clinopyroxene lattice preferred orientations in eclogites

Jérôme Bascou[a,b,*], Andréa Tommasi[a], David Mainprice[a]

[a]*Laboratoire de Tectonophysique, UMR 5568 Université de Montpellier II and CNRS, Place E. Bataillon, F-34095 Montpellier cedex 5, France*
[b]*Instituto de Geociências, Universidade de São Paulo, Rua do Lago, 562, BR-05508-080 São Paulo, Brazil*

Abstract

We use an anisotropic viscoplastic self-consistent (VPSC) model to simulate the development of omphacite lattice preferred orientations (LPOs) in response to deformation by dislocation glide. In these simulations, we consider slip systems identified either in naturally deformed omphacite or in experimentally deformed diopside. Simulated LPOs reproduce very well the characteristic omphacite LPO pattern in naturally deformed eclogites: a strong concentration of [001]-axes sub-parallel to the lineation and of (010)-poles sub-perpendicular to the foliation. These models reconcile the interpretation of omphacite LPOs in eclogites and TEM observations of naturally deformed omphacite, since they show that omphacite LPOs in naturally deformed eclogites may develop by dislocation glide on $1/2\langle110\rangle\{1\bar{1}0\}$, [001]{110} and [001](100). We also investigate the effect of the strain regime on the omphacite LPO development. The simulations show that changes in deformation regime lead to second-order variations in omphacite LPO patterns similar to those observed in eclogites, such as an asymmetry of the LPO relative to the structural frame, a stronger concentration of the [001]-axes relative to the (010)-pole concentration, or a dispersion of [001]-axes in the foliation plane. This suggests that omphacite LPO patterns may carry information on the deformation regime (simple shear, transtension…) active during the high-pressure events. © 2002 Elsevier Science Ltd. All rights reserved.

Keywords: Lattice preferred orientations; Deformation; Dislocation glide

1. Introduction

Clinopyroxene is a major mineralogical constituent of the oceanic crust and upper mantle. Analysis of lower crustal sections (e.g. the Ivrea Zone, Northern Italy; Fountain and Salisbury, 1981; Pin and Sills, 1986) and xenoliths (Halliday et al., 1993) shows that clinopyroxene is also concentrated in mafic granulites and gabbroic intrusions of the lowermost crust. Such mafic rocks are transformed in eclogites by high- (or ultra-high) pressure metamorphism in subduction and/or collision zones. Clinopyroxene omphacite as the major and most deformable constituent of eclogites may then be a key mineral to decipher the tectonic processes active during the high-pressure event.

An important effect of the plastic deformation of rocks is the development of a lattice preferred orientation (LPO) of their constituent minerals (Nicolas and Poirier, 1976). When one slip system is predominant during deformation (e.g.

[100](010) for olivine at high-temperature conditions), the preferred orientation of the slip direction and the slip plane tend to coincide with the flow direction and the flow plane, respectively (Nicolas and Poirier, 1976; Mainprice and Nicolas, 1989). Thus information on the flow regime can be deduced from the orientation of the slip systems relative to the structural frame. Particularly, in the case of a non-coaxial deformation, the obliquity between the LPO and the X, Y and Z structural axes (X = lineation and Z = normal to the foliation) allows the determination of sense of shear. The majority of LPO measurements for the clinopyroxene group in the literature have been made on omphacites from eclogites. The characteristic LPO of omphacite is marked by a strong concentration of (010)-poles normal to the foliation and of [001]-axes parallel to the lineation (e.g. Boundy et al., 1992; Godard and Van Roermund, 1995; Abalos, 1997; Bascou et al., 2001; Mauler et al., 2001; Pipenbreier and Stöckert, 2001). If one assumes that LPO development is controlled by glide on a single dominant slip system, this LPO suggests a dominant activation of the [001](010) slip system. However, dislocations associated with this slip system are not observed in naturally deformed omphacite. In fact, TEM observations of dislocations in

* Corresponding author. Tel.: +33-4671-43602; fax: +33-4671-43603.
E-mail address: bascou@dstu.univ-montp2.fr (J. Bascou).

omphacites from naturally deformed eclogites (Van Roermund and Boland, 1981; Van Roermund, 1983; Buatier et al., 1991; Godard and Van Roermund, 1995) show that dislocation creep results in dominant activation of the $1/2\langle 110\rangle\{1\bar{1}0\}$, $[001]\{110\}$ and $[001](100)$ slip systems. Based on microstructural observations, Godard and Van Roermund (1995) and Mauler et al. (2001) have proposed that activation of other deformation mechanisms, such as grain boundary migration and diffusive mass transfer or diffusion creep with concomitant anisotropic growth, may reconcile the apparent discrepancy between LPO data and TEM observations.

Deformation experiments also contribute to our understanding of the deformation of clinopyroxenes. Such experiments have been mainly performed on diopside single crystals (Avé Lallemant, 1978; Ingrin et al., 1992; Raterron et al., 1994) or polycrystalline aggregates (Boland and Tullis, 1986; Lavie, 1998; Mauler et al., 2000; Bystricky and Mackwell, 2001). These experiments show that plastic flow of diopside is essentially accommodated by three deformation mechanisms. At low temperature, high strain rate, and high stress, diopside deforms by mechanical twinning on (100) and (001) planes (e.g. Avé Lallemant, 1978). At higher temperature, plastic deformation occurs by dislocation creep or diffusion creep depending on grain size and flow stresses (Lavie, 1998; Bystricky and Mackwell, 2001). Dislocation creep accommodated by an association of dislocation glide and dynamic recrystallization by subgrain rotation and grain boundary migration is dominant in both natural clinopyroxenites (Bystricky and Mackwell, 2001) and synthetic polycrystals deformed by torsion (Mauler et al., 2000). In addition, single crystal deformation experiments at moderate and high temperatures show that plastic deformation of diopside results in dominant activation of {110} and (100) slip systems. Between 800 and 900°C, $[001](100)$ is the easiest system with a flow stress on the order of 60 MPa at laboratory strain rates, $[100](010)$ and $1/2\langle 110\rangle\{1\bar{1}0\}$ are less easily activated (flow stresses are on the order of 200 MPa), and $[001]\{110\}$ systems are hard to activate (Ingrin et al., 1992). At higher temperatures (above 1000°C), the activation of $1/2\langle 110\rangle\{1\bar{1}0\}$ slip systems is favored (Ingrin et al., 1991; Raterron et al., 1994).

Slip systems observed in omphacite and diopside are similar. However, rheological laws obtained for diopside aggregates suggest that unreasonable high stresses and/or low strain rates are needed to deform clinopyroxene-rich rocks by dislocation creep at temperatures below 700°. This is in contradiction to microstructural and thermobarometric data in eclogites that indicate that omphacite deforms by dislocation creep at temperatures as low as 450°C (e.g. Buatier et al., 1991; Philippot and Van Roermund, 1992; Pipenbreier and Stöckert, 2001). Indeed, preliminary experimental data on synthetic jadeite polycrystals (Renner, unpublished, cited in Stöckert and Renner, 1998) show low flow stresses, in agreement with the low

melting point of sodic clinopyroxenes (jadeite, omphacite) compared with diopside (Pipenbreier and Stöckert, 2001).

In order to investigate the deformation mechanisms that could produce the observed clinopyroxene LPOs, we use a viscoplastic self-consistent model (VPSC) to simulate the omphacite LPO development in response to deformation by dislocation glide. In these models, we consider that omphacite deforms by slip on those systems identified in naturally deformed eclogites or in experimentally deformed diopside. To investigate the effect of strain regime on the LPO pattern, we modeled omphacite LPO development in simple shear, axial compression, transpression and transtension. Modeled LPO patterns are then compared with omphacite LPO patterns of eclogites sampled in various orogenic domains.

2. Naturally deformed omphacite LPO

2.1. Previous data on clinopyroxene LPOs

Clinopyroxene LPOs have been, up to now, essentially measured on 5-axes universal stage (e.g. Helmstaedt et al., 1972; Van Roermund, 1983; Boundy et al., 1992; Barruol and Mainprice, 1993; Godard and Van Roermund, 1995; Abalos, 1997) and, more recently, using the electron back-scattered diffraction (EBSD) technique (Bascou et al., 2001; Mauler et al., 2001; Pipenbreier and Stöckert, 2001). The most common omphacite LPO is the '(010) fabric' that is characterized by a concentration of (010)-poles and [001]-axes perpendicular to the foliation and parallel to the lineation, respectively. Variations on the relative concentration of (010)-poles and [001]-axes in this characteristic LPO have been traditionally interpreted in terms of strain symmetry during high-pressure deformation (Helmstaedt et al., 1972; Godard and Van Roermund, 1995; Abalos, 1997). Two end-members are described: the 'L-type or constriction fabric', characterized by (010)-poles in a girdle perpendicular to the lineation and [001]-axes forming a single maximum strongly concentrated in the lineation and the 'S-type or flattening fabric', characterized by a strong (010)-poles concentration perpendicular to the foliation and [001]-axes lying in the foliation plane. These end-member fabrics correspond to coaxial-deformation regimes. However, omphacite LPO patterns asymmetric to the X, Y and Z structural axes have also been observed in naturally deformed eclogites (Boundy et al., 1992; Abalos, 1997; Bascou et al., 2001).

The '(100) fabric' characterized by (100)-poles concentrated perpendicular to the foliation, (010)-poles close to the Y-axis, and [001]-axes parallel to the lineation that is common for orthopyroxene (e.g. Mockel, 1969) is rarely described for clinopyroxene. Such LPO patterns were nevertheless observed in an annealed mylonitic eclogite from the Monviso, western Alps (Philippot and Van Roermund, 1992) and in both a mylonitic pyroxenite and

a mylonitic clinopyroxene–garnet amphibolite from the Snowbird tectonic zone, Canada (Ji et al., 1993). LPOs intermediate between the (010) and the (100) fabrics have also been described in eclogites (see Godard and Van Roermund, 1995; Abalos, 1997) as well as a clinopyroxene fabric characterized by [001]-axes concentrated close to the *Y*-axis (Siegesmund et al., 1989; Ji et al., 1993).

2.2. Measured omphacite LPOs

We measured omphacite LPOs of 12 eclogites coming from orogenic domains of contrasting age and geodynamic evolution. The geological setting, microstructures, LPOs and seismic properties of these samples are described in detail in Bascou et al. (2001). For this study, we have selected four of these samples, which display strong and typical LPOs. These four samples (AB.E, B6, SL50, S522) are characterized by different *P*–*T* conditions of eclogitization. Sample AB.E has been collected within the eclogite boudin surrounding the Alpe Arami peridotite massif in the western Alps, north of the Insubric line; pressure and temperature conditions of the eclogitic meta-morphism have been estimated to be above 1.8 GPa and 750–900°C (Heinrich, 1986). Eclogite B6 was sampled in the core of an eclogite boudin located in the Western Gneiss Region (western Norway), north of the Nordfjord–Sogn detachment. Sample SL50 comes from the Sulu region, eastern China; the eclogitic metamorphism conditions were evaluated at ca. 700–890°C and above 2.8 GPa (Zhang et al., 1995). Sample S522 is an eclogitic meta-sediment from the internal nappes of the Gourma area, northern Mali. Coesite relics in omphacite (Caby, 1994) indicate subduction of these rocks up to depths over 100 km (Jahn et al., 2001). These four samples display well-preserved eclogite facies parageneses. The most important constituent minerals are omphacite and garnet; these two mineral phases represent more than 75% of the modal content. All samples exhibit a strong foliation and lineation defined by the shape-preferred orientation of the omphacite crystals. Omphacite grain sizes vary from ca. 0.3 mm in sample S522 to ca. 4 mm in sample AB.E. Garnet grains are almost euhedral with grain sizes up to 2 mm (sample B6).

Omphacite lattice preferred orientations were measured using a scanning electron microscope (SEM) equipped with an EBSD system. The EBSD technique (e.g. Venables and Harland, 1973; Adams et al., 1993) is based on the auto-matic analysis of diffraction patterns (Kikuchi bands) generated in the SEM by interaction of a vertical electron beam with a carefully polished thin section tilted to 70°. The Kikuchi patterns are collected on a phosphor screen, imaged by a low-light, high-resolution CDD camera, and indexed using the CHANNEL + software from HKL Technology. At each point of measurement, the full crystallographic orientation, described by the Euler angles ($\vartheta 1$, ϕ, $\vartheta 2$) is determined with a precision of 1° (Krieger Lassen, 1996).

LPOs of the samples AB.E, B6 and S522 were measured in manual mode and SL50 in automatic mode. For the auto-matic acquisition, measurements are performed on a square grid with a step of the same order as the omphacite grain size of the studied sample (1 mm for SL50).

The measured omphacite LPOs (Fig. 1) are presented on equal area, lower hemisphere stereographic projections in the structural (*X*, *Y*, *Z*) reference frame. Foliation (*XY* plane) is vertical E–W and the lineation (*X* direction) is horizontal in this plane. The fabric strength is expressed by the dimen-sionless texture index *J* (Bunge, 1982). The *J*-index ranges from 1 (random LPO) to infinity (single crystal). However, in our calculations, the *J*-index has an upper bound of ca. 250 because the spherical harmonic series expansion is truncated at degree 22. All samples display typical omphacite LPO patterns characterized by a strong concen-tration of [001]-axes and (010)-poles parallel to the *X*-axis and normal to the *XY* plane, respectively. (110)-poles and [100]-axes are poorly oriented. (110)-poles tend neverthe-less to concentrate in a girdle perpendicular to the lineation with two maxima between the *Y*- and *Z*-axis. [100]-axes display a weak concentration close to the *Y*-axis. Besides these general features, second-order variations in the LPO pattern are observed sample to sample. Sample S522 is distinguishable from the other samples by a stronger concentration of (010)-axes normal to the foliation and a dispersion of [001]-axes in the foliation plane. Samples AB.E, B6 and SL50 are characterized by stronger fabrics; their *J*-indexes range from 6.4 (AB.E) to 7.7 (B6). Both [001]-axes and (010)-poles are very concentrated and are oblique to the structural reference frame. However, in samples B6 and SL50, the [001]-axes are about twice more concentrated than the (010)-poles whereas the [001]-axes and (010)-poles in sample AB.E are characterized by similar maximum densities.

3. Viscoplastic self-consistent modeling of omphacite LPOs

We investigated the evolution of omphacite LPOs using the anisotropic viscoplastic self-consistent model (VPSC) developed by Molinari et al. (1987) and extended to aniso-tropic materials by Lebensohn and Tomé (1993). Recently, this code has been successfully applied to polycrystalline ice (Castelnau et al., 1996) and olivine (Tommasi et al., 2000).

The VPSC model is based on two assumptions: (i) the crystals that constitute the aggregate deform uniquely by homogeneous intracrystalline slip on selected crystallo-graphic planes (dynamic recrystallization is not taken into account), and (ii) the aggregate behavior may be calculated as an average of the crystals behavior. Locally, from grain to grain, strain and stress are heterogeneous and grains in easy glide orientations deform faster than those in hard orienta-tions. Strain compatibility and stress equilibrium are ensured at the aggregate scale, i.e. the volume averaged
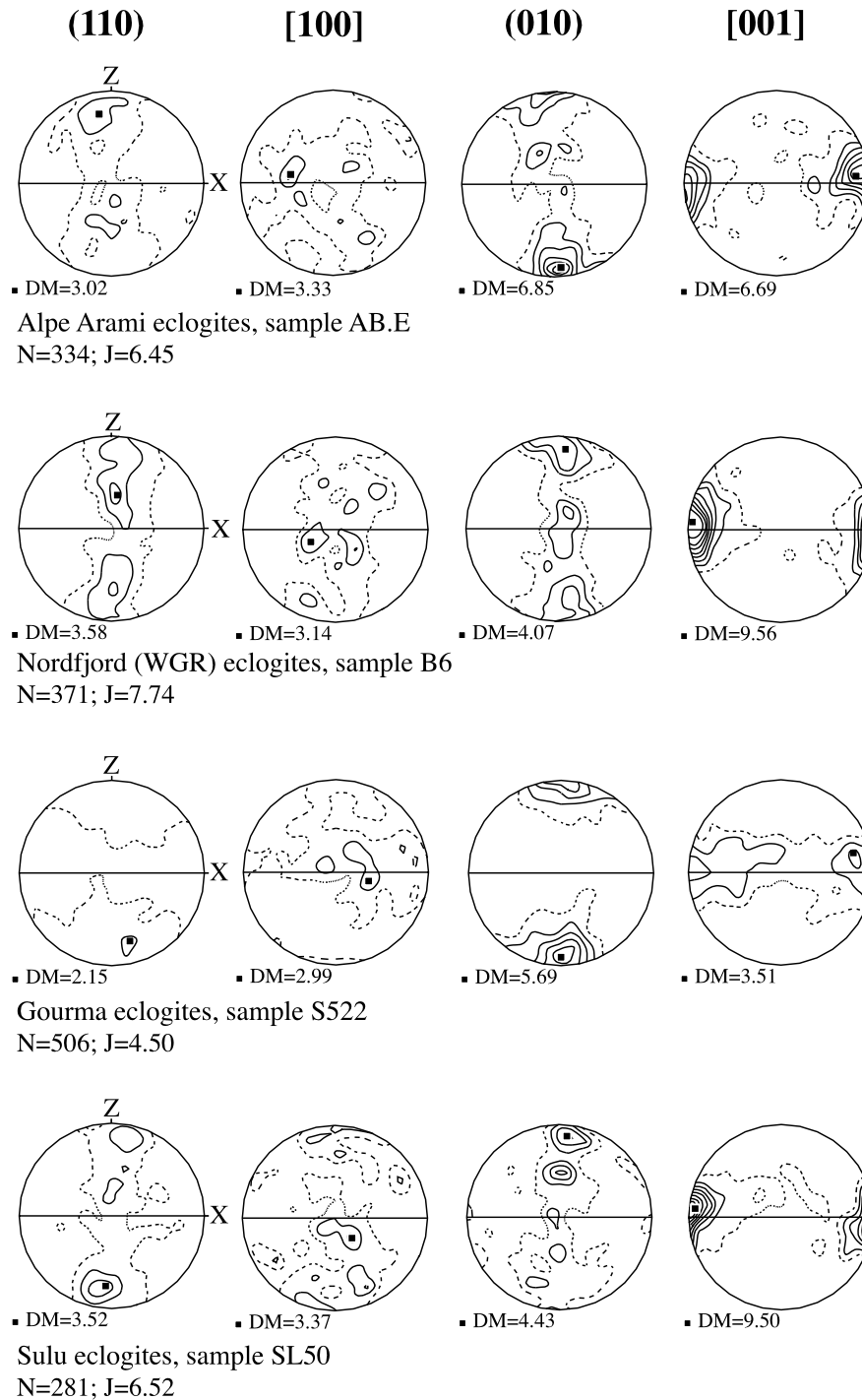
Fig. 1. Omphacite LPO measured using the EBSD technique (Bascou et al., 2001). Equal area projection, lower hemisphere. Equal area projections, lower hemisphere. Contours at 1, 2, 3%... by 1% area. Foliation (*XY* plane; full line) is vertical and lineation (*X*) is horizontal in this plane. *N*: number of measurements. *J*: texture index. *DM*: maximum density.

stresses and strain rates ($\mathbf{s}$, $\dot{\varepsilon}$) of the grains are equal to the polycrystal stress and strain rate ($\bar{\Sigma}$, $\bar{\mathbf{D}}$). The interaction between the grain and the polycrystal is treated using the inclusion formalism of Eshelby (1957), where each grain is handled as an inhomogeneity within a homogeneous effective medium (HEM), which represents the polycrystal. Stresses and strain rates of the grains are thus related to the

macroscopic quantities through:

$$\dot{\varepsilon}_{ij} - D_{ij} = -\alpha \tilde{\mathbf{M}}_{ijkl}\left(s_{kl} - \bar{\Sigma}_{kl}\right) \qquad (1)$$

where $\tilde{\mathbf{M}}$ is the interaction tensor that depends on the rheological properties of the polycrystal and on the shape of the grains. The constant α is used to parameterize the

interaction between grains and the HEM, i.e. to impose more or less stringent kinematic conditions on grains. A zero value of α corresponds to the Taylor (1938) model (the upper bound approach) that imposes homogeneous stress. A value of unity corresponds to the tangent VPSC model of Lebensohn and Tomé (1993), and an infinite value corresponds to the stress equilibrium model (i.e. the lower bound approach; Chastel et al., 1993).

Most models presented below have been performed using the tangent formulation ($\alpha = 1$). Yet microstructural observations in naturally deformed eclogites (e.g. Buatier et al., 1991) as well as in experimentally deformed diopside aggregates (e.g. Mauler et al., 2000) show that deformation of clinopyrexenes in the dislocation creep regime associates dislocation glide and dynamic recrystallization by subgrain rotation and/or grain boundary migration. Thus, considering that during the deformation of omphacite-rich rocks strain compatibility is partly ensured by diffusional processes, we have also performed VPSC simulations in relaxed strain compatibility conditions ($\alpha = 10$). Since LPO patterns produced in coaxial deformation simulations with relaxed strain compatibility conditions ($\alpha = 10$) are similar to those obtained using the tangent formulation ($\alpha = 1$), we will only present LPOs for simple shear models with relaxed compatibility (Fig. 4).

For a given set of slip systems and an initial LPO, the VPSC model calculates the aggregate yield strength (or strain rate), the activity of the slip systems, and the LPO evolution in response to an imposed macroscopic deformation (or stress) history. Slip system data are presented in Table 1. In the model, slip systems of monoclinic omphacite (unit cell parameters: $a = 9.54$ Å, $b = 8.70$ Å, $c = 5.25$ Å and $\beta = 106.06°$ (Bhagat et al., 1992)) are projected into a Cartesian reference frame. Since experimental constraints on the critical resolved shear stresses (CRSS) of the various slip systems of omphacite are lacking, we have investigated the effect of varying the CRSS on the LPO evolution. We

have tested a large range of CRSS values, but since the LPO evolution is weakly dependent on small variations of the CRSS, we only present models for two CRSS sets. CRSS 1 is evaluated from experimental deformation data on diopside single crystals (Ingrin et al., 1992); the CRSS values for all systems are normalized relative to the critical resolved shear stress of the easiest [001](100) system (ca. 60 MPa at laboratory conditions, Ingrin et al., 1992). CRSS 2 is inferred from TEM observations of dislocations in omphacite of naturally deformed eclogites. In this set, the lowest CRSS values (arbitrary equal to one) are affected in those systems whose dislocations are the most frequently observed. The stress exponent n is evaluated from experimental deformation data for diopside single-crystals and polycrystals: values range between 3.3 (Avé Lallemant, 1978; Boland and Tullis, 1986), and 6.5 (Raterron and Jaoul, 1991). Most models were run with $n = 3.5$, but we also performed tests with $n = 5$. Since LPOs predicted in both cases are similar (with only a slightly faster LPO evolution for $n = 5$), we only show here the results for $n = 3.5$.

In the models presented below, an aggregate of 1000 (or 500) omphacite grains, initially spherical and randomly oriented, is deformed in simple shear, axial shortening, transpression and transtension. Each deformation regime is described by a constant velocity gradient tensor L, defined as:

$$L = \begin{bmatrix} 0 & 1 & 0 \\ 0 & 0 & 0 \\ 0 & 0 & 0 \end{bmatrix}, \quad L = \begin{bmatrix} 1 & 0 & 0 \\ 0 & -1 & 0 \\ 0 & 0 & 0 \end{bmatrix},$$

$$L = \begin{bmatrix} 0.5 & 0 & 0 \\ 0 & -1 & 0 \\ 0 & 0 & 0.5 \end{bmatrix}, \quad L = \begin{bmatrix} 0.237 & 1 & 0 \\ 0 & -0.237 & 0 \\ 0 & 0 & 0 \end{bmatrix},$$

$$L = \begin{bmatrix} 0 & 0 & 0 \\ 0 & 0.237 & 0 \\ 0 & 0 & -0.237 \end{bmatrix} \qquad (2)$$

for simple shear, pure shear, axial compression, transpression and transtension simulations, respectively. Transpression and transtension are defined as a combination of simple shear and coaxial deformation. This combination is quantified by the kinematic vorticity number (Wk). In coaxial deformation, $Wk = 0$ and in simple shear $Wk = 1$. Our transpression and transtension models are characterized by $Wk = 0.9$, i.e. by predominance of the simple shear component.

In order to compare the LPO evolution in different deformation regimes, all LPO data are displayed for an equivalent strain of one, obtained by the accumulation of 40 identical deformation steps. The equivalent strain is

Table 1
Slip system data used in the CRSS 1 and CRSS 2 models

Slip systems	CRSS 1[a]	CRSS 2[a]
[001](100)	1	1
[001](110)	10	1
[001]($1\bar{1}0$)	10	1
[$1\bar{1}0$](110)	3	1
[110]($1\bar{1}0$)	3	1
[100](010)	3	8
[001](010)	8	8
[$1\bar{1}2$](110)	10	8
[112]($1\bar{1}0$)	10	8
[010](100)	10	8
[$1\bar{1}\bar{2}$](110)	10	8
[11$\bar{2}$]($1\bar{1}0$)	10	8
[101](010)	10	8

[a] Critical resolved shear stresses (CRSS) are normalized by the $CRSS_{[001](100)}$.
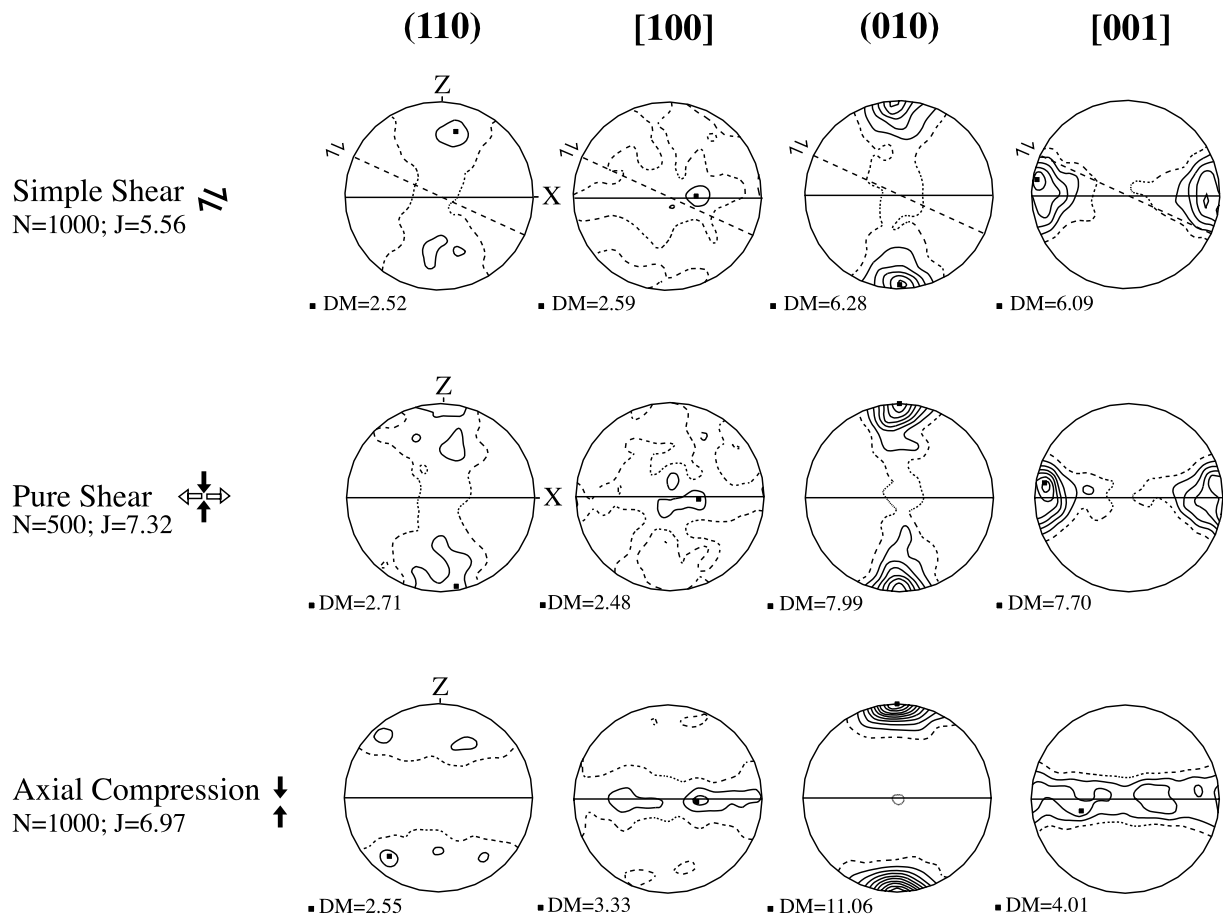
VPSC models with CRSS 1

Fig. 2. Omphacite LPO simulated in VPSC models with $\alpha = 1$ and CRSS evaluated from experimental deformation data on diopside (CRSS 1). Dextral simple shear, pure shear and axial compression at equivalent strain of one. Equal area projections, lower hemisphere. Contours at 1, 2, 3%... by 1% area. Full line: foliation (*XY* plane) is vertical and lineation (*X*) is horizontal. For the model in simple shear ($\gamma = 1.73$), dotted line marks the shear plane and the direction of shear is horizontal in this plane. *N*: number of grains. *J*: texture index. *DM*: maximum density.

defined as (Molinari et al., 1987):

$$\varepsilon_{eq} = \int D_{eq}(\tau)d\tau \qquad (3)$$

where $d\tau$ is the time increment of a deformation step, chosen so that each deformation step leads to a 0.025 equivalent strain for the polycrystal. The Von Mises equivalent strain rate D_{eq} is defined as:

$$D_{eq} = (\tfrac{2}{3}D_{ij}D_{ij})^{1/2} \qquad (4)$$

Although eclogites are composed essentially of omphacite and garnet, we choose to approach the deformation of omphacite in polymineralic eclogites by simulations using 100% omphacite aggregates. This choice is based on microstructural data that suggest that garnet generally behaves as rigid inclusions during eclogite deformation, except at very high temperature (e.g. Ando et al., 1993). This hypothesis is also supported by the random crystallographic orientation of garnet in all but one of the samples

studied by Bascou et al. (2001) and by the lack of correlation between variations in the modal content of garnet and changes in the omphacite LPO. Moreover, previous VPSC simulations of the LPO evolution in two-phase systems, like olivine–enstatite (Wenk et al., 1991) and quartz–mica aggregates (Canova et al., 1992), show that the presence of a hard phase does not change fundamentally the LPO pattern of the soft matrix.

3.1. Simple shear and pure shear

Models in simple shear ($\gamma = 1.73$) and pure shear (Figs. 2 and 3) performed using the tangent formulation ($\alpha = 1$) generate similar LPOs characterized by strong concentrations of (010)-poles and [001]-axes perpendicular to the *XY*-plane and parallel to the *X*-axis, respectively. The (010)-poles systematically display slightly stronger concentrations than the [001]-axes. (110)-poles and [100]-axes are nearly randomly oriented. However, (110)-poles tend to
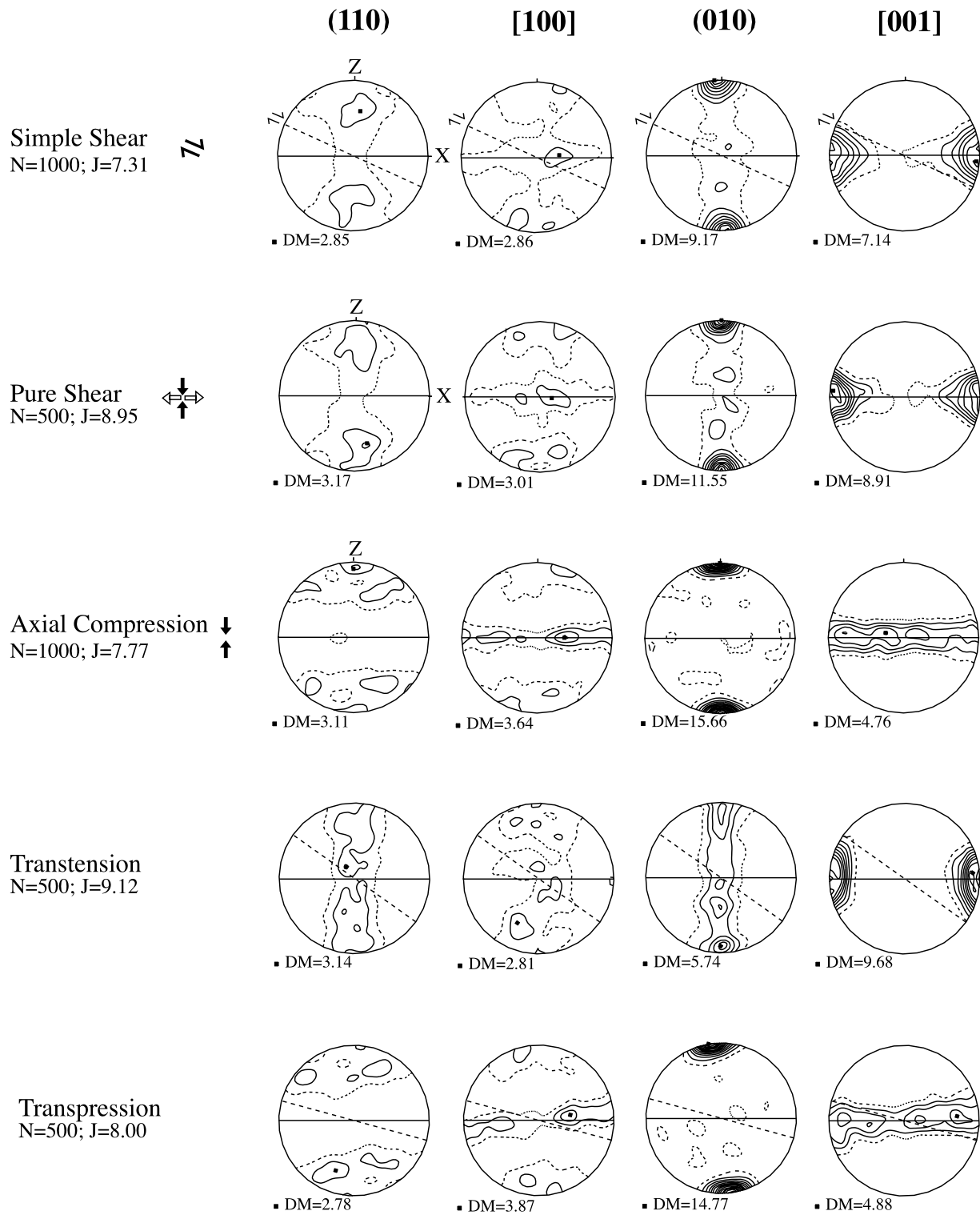
VPSC models with CRSS 2

Fig. 3. Omphacite LPO simulated in VPSC models with $\alpha = 1$ and with CRSS evaluated from TEM observations of dislocations in omphacites of naturally deformed eclogites (CRSS 2). LPO formed in dextral simple shear, pure shear, axial compression, transpression ($Wk = 0.9$), and transtension ($Wk = 0.9$) for an equivalent strain of one. Equal area projections, lower hemisphere. Contours at 1, 2, 3%... by 1% area. Full line: foliation (*XY* plane) is vertical and lineation (*X*) is horizontal. Dotted line: shear plane. *N*: Number of grains. *J*: texture index. *DM*: Maximum density.

VPSC models (α = 10)
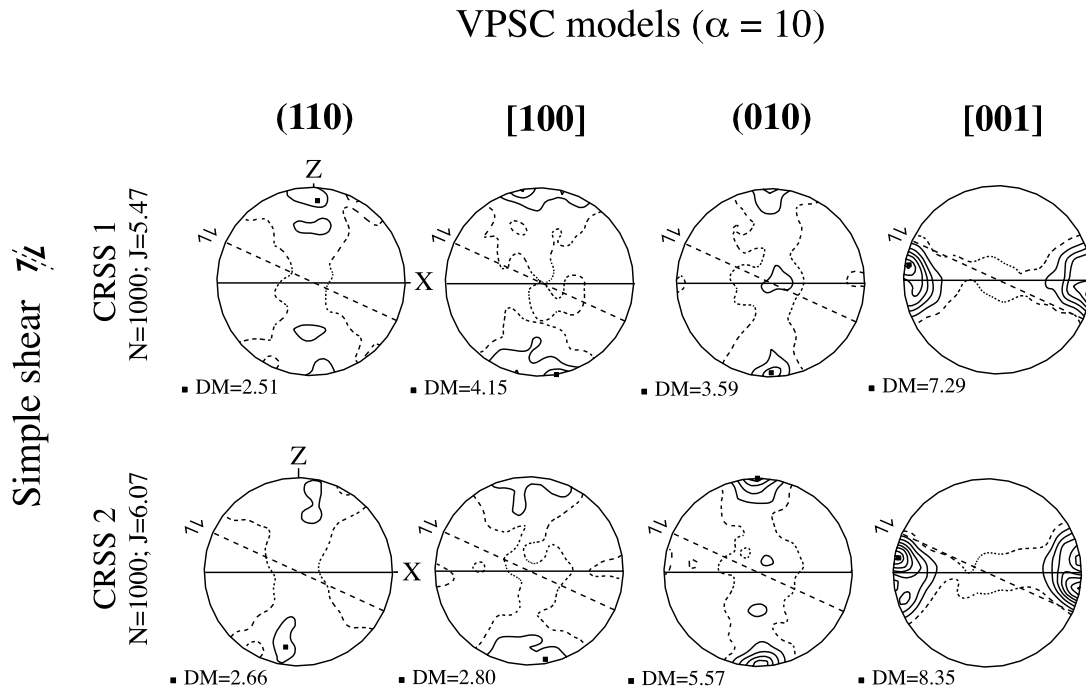
Fig. 4. Omphacite LPO developed in simple shear models with relaxed strain compatibility ($\alpha = 10$). $E_{eq} = 1$ ($\gamma = 1.73$) and dextral sense of shear. Equal area projections, lower hemisphere. Contours at 1, 2, 3%… by 1% area. Full line: foliation (*XY* plane) is vertical and lineation (*X*) is horizontal. Dotted line: shear plane. *N*: Number of grains. *J*: texture index. *DM*: maximum density.

form a girdle perpendicular to the *X*-axis with a weak maximum at ca. 60° to the *XY* plane and [100]-axes display a maximum of density close to the *Y*-axis.

Models performed using critical resolved shear stresses inferred from experimental deformation of diopside (CRSS 1) and from TEM analyses of naturally deformed omphacite (CRSS 2) produce similar LPOs, but the LPO evolution is slightly faster in CRSS 2 models. In simple shear models with relaxed strain compatibility ($\alpha = 10$), the difference between LPOs simulated using the CRSS 1 and CRSS 2 sets become more pronounced. The CRSS 1 model develops a maximum and a sub-maximum of (010)-poles close to the *Z*-axis and the *Y*-axis, respectively, whereas the CRSS 2 model develops a single (010)-maximum close to the *Z*-axis (Fig. 4). In contrast to simulations with $\alpha = 1$, the relaxed CRSS 1 model is characterized by a strong concentration of [100]-axes close to the *Z*-axis and a stronger concentration of [001]-axes relative to the (010)-poles. Finally, both simple shear models with relaxed strain compatibility develop LPO patterns asymmetric relatively to the foliation (*XY*) plane: the [001]-axes are intermediate between the shear direction and the *X*-axis (Fig. 4), in agreement with the imposed dextral shear.

3.2. Axial shortening

Models in axial compression (Figs. 2 and 3) develop LPOs that are symmetrical relative to the *XY* plane. (010)-poles are strongly concentrated close to *Z*, the shortening direction. [001]-axes and [100]-axes are dispersed in the *XY*

plane with a weak maximum of [100] at ca. 20° from the *Y*-axis. (110)-poles are highly dispersed, but display a weak concentration close to the *Z*-axis. As in simple shear, LPOs developed using both CRSS sets are similar and CRSS 2 models produce a stronger concentration of (010)-poles close to the *Z*-axis.

3.3. Transpression and transtension

Models in transpression (*Wk* = 0.9) produce LPO patterns similar to those of axial shortening (Fig. 3). However, in transpression, [001]-axes tend to form a girdle with two maxima at ca. 20° from the *X*-axis and the (010)-poles display significantly higher concentrations than those developed in axial shortening. LPOs formed in transtension models (*Wk* = 0.9) are similar to simple shear ones, but highly oblique to the shear plane and direction. [001]-axes are concentrated in a small circle around the lineation, at 35° to the shear direction. They display the strongest concentration with a maximum density of 9.7%. (010)-poles tend to form a girdle sub-perpendicular to the lineation with a maximum density close to the *Z*-axis. (110)-poles also form a girdle normal to the lineation but their dispersion is higher than the (010)-poles. [100]-axes are still more scattered.

3.4. Slip systems activity

Evolution of the slip systems activity with finite strain in CRSS 1 and CRSS 2 models is displayed in Fig. 5. In simple shear, both models are characterized by dominant activation of [001] systems. In CRSS 1 models, the activity of the
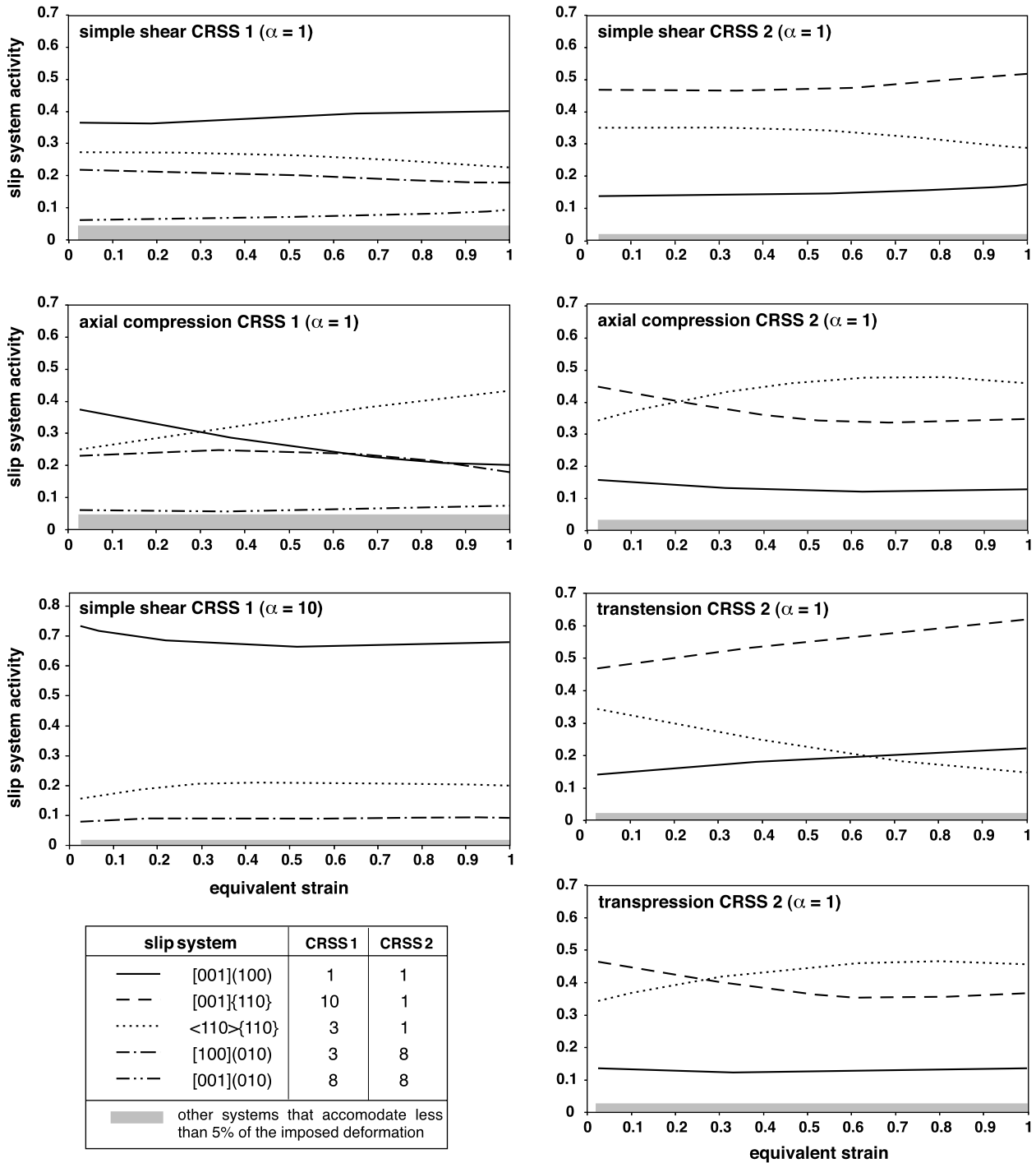
Fig. 5. Evolution of the slip systems activity with finite strain in simple shear, axial compression, transpression, or transtension models using either the CRSS 1 or the CRSS 2 critical resolved shear stresses sets.

[001](100) system, which has the lowest CRSS value, increases with increasing strain, accommodating 40% of the deformation at an equivalent strain of one. Activity of $1/2\langle110\rangle\{1\bar{1}0\}$ and [100](010) decreases with increasing strain, but $1/2\langle110\rangle\{1\bar{1}0\}$ displays a higher activity than [100](010) even though both systems are characterized by a similar CRSS. In CRSS 2 models, the activity of the [001]{110} system increases quickly after an equivalent strain of 0.5. This system accommodates more than 50% of the deformation at an equivalent strain of one ($\gamma = 1.73$). In general, {110} systems accommodate more than 75% of the deformation. The resulting LPO is marked by a strong concentration of [001]-axes sub-parallel to the X-axis and by an orientation of (010)-poles sub-parallel to the Z-axis.

In axial shortening and transpression, the symmetrical

Diopside LPO in sheared gabbro

(100)   **(010)**   **[001]**
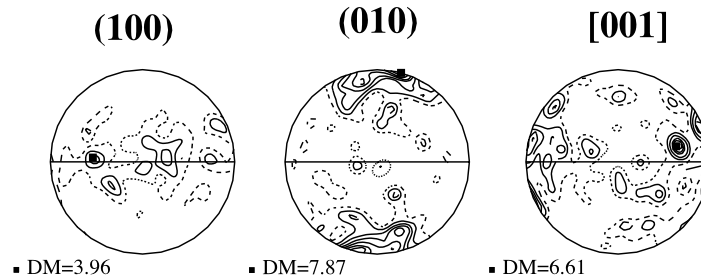
■ DM=3.96   ■ DM=7.87   ■ DM=6.61

Fig. 6. Clinopyroxene LPO in a sheared gabbro from the Ivrea zone (northern Italy; Barruol and Mainprice, 1993). U-stage data; equal area projection, lower hemisphere. Contours at 1 multiple of a uniform distribution intervals. Full line: foliation (*XY* plane) is vertical and lineation (*X*) is horizontal.

$1/2\langle110\rangle\{1\bar{1}0\}$ systems are better adapted to accommodate the imposed deformation geometry. However, in CRSS 2 models, $[001]\{110\}$ is also activated (0.35 at an equivalent strain of 0.4). In transtension, as in simple shear, the $[001]\{110\}$ system displays the highest activity. However, in transtension, the activity of $[001](100)$ increases faster, leading to a higher concentration of [001]-axes than in simple shear.

Relaxation of strain compatibility in simple shear simulation using the CRSS 1 set favors the activity of the $[001](100)$ system. This system accommodates almost 70% of the deformation (Fig. 5). The $1/2\langle110\rangle\{1\bar{1}0\}$ and $[100](010)$ systems accommodate 20 and 10% of the deformation, respectively. Slip on the 'hard' $[001](010)$ is no longer required. In CRSS 2 models the activity of slip systems is similar in simulations with relaxed strain compatibility ($\alpha = 10$) or with more stringent compatibility conditions ($\alpha = 1$).

4. Discussion

Omphacite LPOs simulated using viscoplastic self-consistent models reproduce well the typical omphacite LPOs of naturally deformed eclogites (Fig. 1) as well as diopside LPOs in sheared gabbros of the lower crust (Barruol and Mainprice, 1993; Fig. 6). Both CRSS 1 and CRSS 2 models develop concentrations of (010)-poles and [001]-axes perpendicular to the foliation and parallel to the lineation, respectively. LPOs modeled using the CRSS 2 set are characterized by the strongest concentration of (010)-poles, even though (010) systems are not activated. Moreover, even in CRSS 1 models, $[h01](010)$ systems accommodate less than 25% of the imposed deformation (Fig. 5). This suggests that the orientation of omphacite (010)-planes parallel to the foliation observed in eclogites is correlated to the activity of {110} systems. During the deformation, the omphacite crystal rotates toward a position in which the resolved shear stress on the two {110} equivalent planes will be equal and the highest. For geometrical reasons, ({110} is bisector of (100) and (010)), this position is reached with either the (010) plane or the (100) plane

parallel to the foliation (Fig. 7). The orientation with the (010) plane parallel to the foliation is preferred due to the monoclinic symmetry of omphacite. Indeed, in omphacite, the angle between (110) and ($\bar{1}$10) planes is different by 90° (95° for omphacite crystals of unit cell parameters: $a = 9.54$ Å, $b = 8.70$ Å, $c = 5.25$ Å; Fig. 7), and this results in higher resolved shear stresses on {110} planes when the crystal is oriented with (010) parallel to the foliation. This strong relation between the crystallographic structure and the concentration of (010)-poles normal to the foliation is supported by the LPO predicted in a simple shear with a model crystal structure with unit cell parameters: $a = 8.70$ Å, $b = 9.54$ Å, $c = 5.25$ Å and (110):($\bar{1}$10) $\sim 85°$, i.e. with an inversion of a and b unit cell parameters relative to the omphacite crystal. In fact, this model produces a concentration of [100]-axes perpendicular to the foliation. The high activity of slip on {110} planes (Fig. 5) may also explain the similarity of LPOs formed in the two models (CRSS 1 and CRSS 2). Although the easiest slip systems in these models differ, glide on the {110} planes is geometrically necessary unless the strain is relaxed. Indeed, in models with relaxed strain compatibility, LPOs developed in CRSS 1 and CRSS 2 models vary.

The good agreement between measured and modeled omphacite LPOs also suggests that our simulations using pure omphacite aggregates offer a good approximation of the natural deformation of omphacite in polymineralic eclogites. Besides the excellent first-order agreement
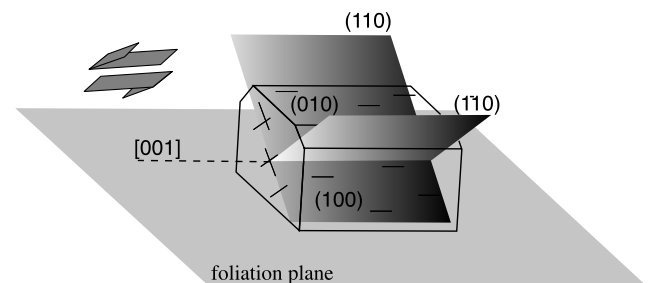
Fig. 7. Schematic diagram showing the omphacite crystal in the position in which the resolved shear stress on the two {110} equivalent planes is the highest. Omphacite unit cell parameters: $a = 9.54$ Å, $b = 8.70$ Å, $c = 5.25$ Å; (110):($\bar{1}$10) $\sim 95°$.

between measured and modeled clinopyroxene LPOs, we may also reproduce the different omphacite LPOs observed in naturally deformed eclogites by varying the deformation regime in the simulations. Omphacite LPOs predicted by models in simple shear and pure shear are characterized by strong (010) and [001] single maxima normal to the foliation and parallel to the lineation, respectively. A similar LPO is observed in many naturally deformed eclogites, such as AB.E (Fig. 1). Axial shortening and transpression models are characterized by a very strong concentration of (010)-poles perpendicular to the foliation and a girdle distribution of [001]-axes in the foliation. For low amounts of pure shear ($Wk = 0.9$), transpression models develop a weak maximum of [001] close to the lineation, but for higher amounts of pure shear ($Wk = 0.75$) the [001]-axes maximum is rotated towards the Y-axis. Simulated LPOs developed in transpressive regimes with low amounts of pure shear reproduce well the LPOs of the Gourma S522 sample (Fig.1). Finally, models in transtension show that, at low proportions of pure shear relative to the simple shear component ($Wk = 0.9$), both (010) and [001] form single maxima, but [001]-axes develop higher concentrations than (010)-poles. Similar patterns are also observed in simple shear models with relaxed strain compatibility, but these later also develop a clear obliquity between the [001]-axes concentration and the lineation, which suggests that non-coaxial strain may produce the obliquity observed in natural samples. This LPO is the most common pattern in naturally deformed eclogites studied by Bascou et al. (2001), e.g. the Sulu (SL50) and the Western Gneiss Region (B6) samples (Fig. 1). It is interesting to note that recent tectonic studies (Krabbendam and Dewey, 1998) propose that transtension played an important role in the exhumation of ultra-high pressure rocks in the Western Gneiss Region.

5. Conclusion

The good agreement between omphacite LPOs measured in naturally deformed eclogites and the LPOs developed in VPSC models using various deformation regimes suggests that:

- Omphacite LPO typical of naturally deformed eclogites can be generated during plastic deformation by slip on $1/2\langle 110\rangle\{1\bar{1}0\}$, $[001]\{110\}$ and $[001](100)$ systems. Dominant activation of these slip systems is in agreement with TEM studies in naturally deformed omphacites and high-temperature, high-pressure experimental deformation data for diopside. In addition, for omphacite, the models show that slip on {110} planes plays a major role on the orientation of (010)-poles normal to the foliation. A similar effect is expected for diopside, because its unit cell parameters are similar to those of omphacite and {110} slip systems are easily activated under moderate to high-temperature conditions.

- Second-order variations of omphacite LPO patterns observed in naturally deformed eclogites are probably related to variations in the deformation regimes active under eclogite–facies conditions. For instance, the asymmetry of omphacite LPO in samples B6 (WGR), AB.E (Alpe Arami) and SL50 (Sulu) may indicate non-coaxial strain during the eclogitic deformation. Thus LPO patterns of omphacite deformed under eclogite facies conditions may be a good tool to constrain some of the tectonic processes active during the high-pressure deformation of eclogites.

References

Abalos, B., 1997. Omphacite fabric variation in the Cabo Ortegal eclogite (NW Spain): relationship with strain symmetry during high-pressure deformation. Journal of Structural Geology 19, 621–637.

Adams, B.I., Wright, S.I., Kunze, K., 1993. Orientation imaging: the emergence of a new microscopy. Metallurgical Transactions 24A, 819–831.

Ando, J.I., Fujino, K., Takeshita, T., 1993. Dislocation microstructures in naturally deformed silicate garnets. Physics of the Earth and Planetary Interiors 80, 105–116.

Avé Lallemant, H.G., 1978. Experimental deformation of diopside and websterite. Tectonophysics 48, 1–27.

Barruol, G., Mainprice, D., 1993. 3D seismic velocities calculated from LPOs and reflectivity of a lower crustal section—example of the Val Sesia (Ivrea Zone, Northern Italy). Geophysical Journal International 115, 1169–1188.

Bascou, J., Barruol, G., Vauchez, A., Mainprice, D., Egydio-Silva, M., 2001. EBSD-measured lattice preferred orientations and seismic properties of eclogites. Tectonophysics 342, 61–80.

Bhagat, S.S., Bass, J.D., Smyth, J.R., 1992. Single-crystal elastic properties of omphacite-C2/c by Brillouin spectroscopy. Journal of Geophysical Research 97, 6843–6848.

Boland, J.N., Tullis, T.E., 1986. Deformation behavior of wet and dry clinopyroxenite in the brittle to ductile transition region. In: Hobbs, B.E., Heard, H.C. (Eds.), Mineral and Rock Deformation: Laboratory Studies. American Geophysical Union Geophysical Monograph 36, pp. 35–49.

Boundy, T.M., Fountain, D.M., Austrheim, H., 1992. Structural

development and petrofabrics of eclogite facies shear zones, Bergen Arcs, western Norway: implications for deep crustal deformational processes. Journal of Metamorphic Geology 10, 127–146.

Buatier, M., Van Roermund, H.L.M., Drury, M.R., Lardeaux, J.M., 1991. Deformation and recrystallization mechanisms in naturally deformed omphacites from the Sesia–Lanzo zone; geophysical consequences. Tectonophysics 195, 11–27.

Bunge, H.J., 1982. Texture Analysis in Materials Sciences. Butterworths, London.

Bystricky, M., Mackwell, S., 2001. Creep of dry clinopyroxene aggregates. Journal of Geophysical Research 106, 13443–13454.

Caby, R., 1994. Precambrian coesite from northern Mali: first record and implications for plate tectonics in the trans-Saharan segment of the Pan-African belt. European Journal of Mineralogy 6, 235–244.

Canova, G.R., Wenk, H.R., Molinari, A., 1992. Deformation modelling of multi-phase polycrystals: case of a quartz–mica aggregate. Acta Metallurgica et Materialia 40, 1519–1530.

Castelnau, O., Duval, P., Lebensohn, R.A., Canova, G.R., 1996. Visco-plastic modeling of texture development in polycrystalline ice with a self-consistent approach: comparison with bound estimates. Journal of Geophysical Research 101, 13851–13868.

Chastel, Y.B., Dawson, P.R., Wenk, H.-R., Bennet, K., 1993. Anisotropic convection with implications for the upper mantle. Journal of Geophysical Research 98, 17757–17771.

Eshelby, J.D., 1957. The determination of the elastic field of an ellipsoidal inclusion, and related problems. Proceedings of the Royal Society of London A 241, 376–396.

Fountain, D.M., Salisbury, M.H., 1981. Exposed cross-sections through the continental crust: implication for crustal structure, petrology and evolution. Earth and Planetary Science Letters 56, 263–277.

Godard, G., Van Roermund, H.L.M., 1995. Deformation-induced clino-pyroxene from eclogites. Journal of Structural Geology 17, 1425–1443.

Halliday, A.N., Dickin, A.P., Hunter, R.N., Davies, G.R., Dempster, T.J., Hamilton, P.J., Upton, B.G.J., 1993. Formation and composition of the lower continental crust: evidence from Scottish xenolith suites. Journal of Geophysical Research 98, 581–607.

Heinrich, C.A., 1986. Eclogite facies regional metamorphism of hydrous mafic rocks in the Central Alpine Adula Nappe. Journal of Petrology 27, 123–154.

Helmstaedt, H., Anderson, O.L., Gavasci, A.T., 1972. Petrofabric studies of eclogite, spinel–websterite, and spinel–lherzolite xenoliths from kimberlite-bearing breccia pipes in southeastern Utah and northeastern Arizona. Journal of Geophysical Research 77, 4350–4365.

Ingrin, J., Doukhan, N., Doukhan, J.C., 1991. High-temperature deformation of diopside single crystals. 2, TEM investigation of the induced defect microstructures. Journal of Geophysical Research 96, 1428–14297.

Ingrin, J., Doukhan, N., Doukhan, J.C., 1992. Dislocation glide systems in diopside single crystals deformed at 800–900°C. European Journal of Mineralogy 4, 1291–1302.

Jahn, B., Caby, R., Monié, P., 2001. The oldest UHP eclogites of the world: age of UHP metamorphism, nature of protoliths and tectonic implications. Chemical Geology 178, 143–158.

Ji, S., Salisbury, M., Hanmer, S., 1993. Petrofabric, P-wave anisotropy and seismic reflectivity of high-grade tectonites. Tectonophysics 222, 195–226.

Krabbendam, M., Dewey, F., 1998. Exhumation of UHP rocks by trans-tension in the Western Gneiss Region, Scandinavian Caledonides. In: Holdsworth, R.E., Strachan, R.A., Dewey, J.F. (Eds.), Continental Transpressional and Transtensional Tectonics. Geological Society of London, Special Publication 135, pp. 159–181.

Krieger Lassen, N.C., 1996. The relative precision of crystal orientations measured from electron backscattering patterns. Journal of Microscop 181, 72–81.

Lavie, M.P., 1998. Déformation expérimentale du diopside polycristallin. Ph.D. thesis, Paris XI Orsay.

Lebensohn, R.A., Tomé, C.N., 1993. A self-consistent anisotropic approach for the simulation of plastic deformation and texture development of polycrystals: application to zirconion alloys. Acta Metallurgica et Materialia 41, 2611–2624.

Mauler, A., Bystricky, M., Kunze, K., Mackwell, S., 2000. Microstructure and lattice preferred orientations in experimentally deformed clino-pyroxene aggregates. Journal of Structural Geology 22, 1633–1648.

Mauler, A., Godard, G., Kunze, K., 2001. Crystallographic fabrics of omphacite, rutile and quartz in Vendee eclogites (Armorican Massif, France). Consequences for deformation mechanisms and regimes. Tectonophysics 342, 81–112.

Mockel, J.R., 1969. The structural petrology of the garnet peridotite of Alpe Arami (Ticino, Switzerland). Leidse Geologische Mededlingen 42, 61–130.

Molinari, A., Canova, G.R., Azhy, S., 1987. A self-consistent approach of the large deformation polycrystal viscoplasticity. Acta Metallurgica 35, 2983–2994.

Nicolas, A., Poirier, J.P., 1976. Crystalline Plasticity and Solid State Flow in Metamorphic Rocks. Wiley, New York.

Philippot, P., Van Roermund, H.L.M., 1992. Deformation processes in eclogitic rock: evidence for the rheological delamination of the oceanic crust in deeper levels of subduction zones. Journal of Structural Geology 14, 1059–1077.

Pipenbreier, D., Stöckert, B., 2001. Plastic flow of ompfacite in eclogites at temoperatures below 500°C—implications for interplate coupling in subduction zones. International Journal of Earth Sciences 90, 197–210.

Pin, C., Sills, J.D., 1986. Petrogenesis of layered gabbros and ultramafic rocks from Val Sesia, NW Italy: trace elements and isotope geo-chemistry. In: Dawson, J.B., Carswell, D.A., Hall, J., Wedepohl, K.H. (Eds.), The Nature of the Continental Crust. Geological Society Special Publication 24, pp. 231–249.

Raterron, P., Jaoul, O., 1991. High-temperature deformation of diopside single crystal. 1, Mechanical data. Journal of Geophysical Research 96, 14277–14286.

Raterron, P., Doukhan, N., Jaoul, O., Doukhan, J.C., 1994. High tempera-ture deformation of diopside IV: predominance of {110} glide above 1000°C. Physics of the Earth and Planetary Interiors 82, 209–222.

Siegesmund, S., Takeshita, T., Kern, H., 1989. Anisotropy of Vp and Vs in an amphibolite of the deeper crust and its relationship to the mineral-ogical, microstructural and textural characteristics of the rock. Tectono-physics 157, 25–38.

Stöckert, B., Renner, J., 1998. Rheology of crustal rocks at ultra-high pressure. In: Hacker, B.R., Liou, J.G. (Eds.). When Continents Collide: Geodynamics and Geochemistry of Ultrahigh-pressure Rocks. , pp. 57–95.

Taylor, G.I., 1938. Plastic strain in metals. Journal of the Institute of Metals 62, 301–324.

Tommasi, A., Mainprice, D., Canova, G., Chastel, Y., 2000. Viscoplastic self-consistent and equilibrium-based modeling of olivine lattice preferred orientations. Implications for upper mantle seismic aniso-tropy. Journal of Geophysical Research 105, 7893–7908.

Van Roermund, H.L.M., 1983. Petrofabrics and microstructures of ompha-cites in a high temperature eclogite from the Swedish Caledonides. Bulletin de Minéralogie 106, 709–713.

Van Roermund, H.L.M., Boland, J.N., 1981. The dislocation substructures of naturally deformed omphacites. Tectonophysics 78, 403–418.

Venables, J.A., Harland, C.J., 1973. Electron back-scattering patterns—a new technique for obtaining crystallographic information in the scan-ning electron microscope. Philosophical Magazine 27, 1193–1200.

Wenk, H.-R., Bennet, K., Canova, G.R., Molinari, A., 1991. Modelling plastic deformation of peridotite with the self-consistent theory. Journal of Geophysical Research 96, 8337–8349.

Zhang, R.Y., Hirajima, T., Banno, S., Cong, B., Liou, J.G., 1995. Petrology of ultrahigh-pressure rocks from the southern Su–Lu region, eastern China. Journal of Metamorphic Geology 13, 659–675.

Erratum to "Plastic deformation and development of clinopyroxene lattice preferred orientations in eclogites"☆
[Journal of Structural Geology 24 (2002) 1357–1368]

Jérôme Bascou[a,b,*], Andréa Tommasi[a], David Mainprice[a]

[a]*Laboratoire de Tectonophysique, UMR 5568, Université de Montpellier II and CNRS, Place E. Bataillon, F-34095, Montpellier cedex 5, France*
[b]*Instituto de Geociências, Universidade de São Paulo, Rua do Lago 562, Cep: BR-05508-080 São Paulo, Brazil*

The following are the correct versions of Eq. (1) and the last part of Eq. (2), i.e. the velocity gradient tensor for transtension simulations of the above paper:

$$\dot{\varepsilon}_{ij} - D_{ij} = -\alpha \tilde{M}_{ijkl}\left(s_{kl} - \sum_{kl}\right) \tag{1}$$

$$L = \begin{bmatrix} 0 & 1 & 0 \\ 0 & 0.237 & 0 \\ 0 & 0 & -0.237 \end{bmatrix} \tag{2}$$

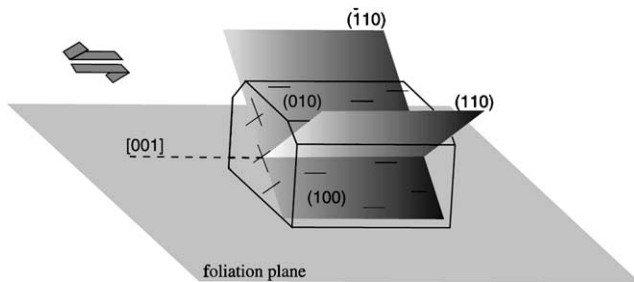The correct version of Fig. 7 is published here.

Fig. 7. Schematic diagram showing the omphacite crystal in the position in which the resolved shear stress on the two {110} equivalent planes is the highest. Omphacite unit cell parameters: $a = 9.54$ Å, $b = 8.70$ Å, $c = 5.25$ Å; (110):($\bar{1}$10) ~ 95°.

On page 1359 the last sentence of the left hand column should read as follows:

At each point of measurement, the full crystallographic orientation, described by the Euler angles ($\varphi 1$, φ, $\varphi 2$) is determined with a precision better than 1° (Krieger Lassen, 1996).

Below is an additional reference that should have been included in this article:

Mainprice, D., Nicolas A., 1989. Development of shape and lattice preferred orientations: application to the seismic anisotropy of the lower crust. Journal of Structural Geology 11, 175–199.

The Publisher would like to apologize for any problems or confusion that may have arisen due to these oversights.

☆ PII of original article S0191-8141(01)00137-7.

* Corresponding author. Tel.: +33-4671-43602; fax: +33-4671-43603.
E-mail address: bascou@dstu.univ-montp2.fr (J. Bascou).